

## **A Parametric Study of Air-Water Countercurrent Flow Limitation in a Horizontal Pipe Connected to an Inclined Riser**

**Seong-Kwon Kang, In-Cheol Chu, Hee Cheon NO, and Moon-Hyun Chun**

Korea Advanced Institute of Science and Technology  
373-1, Kusong-Dong, Yusong-Gu, Taejon, 305-701, Korea

**Chang-Kyung Sung and Sang-Jun Ha**

Korea Electric Power Research Institute  
103-16, Moonji-dong, Yusong-Gu, Taejon, 305-380, Korea

### **ABSTRACT**

*An experimental investigation has been performed to examine the effects of various geometrical parameters on the air-water countercurrent flow limitation (CCFL) in a simulated PWR hot leg. A total of 103 experimental data for the onset of CCFL and zero liquid penetration have been obtained for various combinations of test parameters. It is observed that the CCFL can be classified into three different categories: ① the onset of CCFL, ② the partial liquid delivery, and ③ the zero liquid penetration. The observed mechanisms of CCFL were different depending on the inlet water flow rate. The effect of pipe diameter on the onset of CCFL for short horizontal pipes is not evident. For longer horizontal pipes with a small pipe diameter, however, air flow rates to initiate the onset of CCFL are much smaller than those with a larger pipe diameter when the inlet water flow rate is fixed. The effects of horizontal pipe length and that of horizontal pipe length-to-diameter ( $L/D$ ) ratio on CCFL are about the same, and a longer horizontal pipe length (or a larger  $L/D$  ratio) leads to lower velocities of air and water for the onset of air-water CCFL.*

### **1. INTRODUCTION**

The phenomenon of countercurrent flooding has already been extensively studied for more than 30 years both experimentally and theoretically, but most of the existing studies on flooding were focused on vertical (Wallis, 1969; Kutateladze, 1972) and horizontal (Wallis et al., 1973; Gardner, 1983; Choi et

al., 1995) pipes with a small diameter of less than 0.10 m. More recently, however, the countercurrent flooding in various pipe geometry, such as (1) vertical-to-horizontal, (2) vertical-to-inclined pipes containing elbows of varying angles, and (3) horizontal tube connected to an inclined riser (Ohnuki, 1986; Siddiqui et al., 1986; Kawaji et al., 1991; Wongwises, 1996) has also been investigated. The geometry of the bend that connects the horizontal pipe to an inclined riser, in particular, is analogous to that of a hot leg connecting the pressure vessel with the steam generator in a pressurized water reactor (PWR).

In connection with the safety analysis of nuclear reactor systems, the most typical events where the countercurrent flow limitation (CCFL) can occur in the hot legs of PWRs are the reflood phase of a large break LOCA and the reflux cooling in a small break LOCA.

The main purpose of this work is to investigate the characteristics of CCFL in a horizontal pipe connected to an inclined riser by a 35 degree bend, which simulates the geometry of a PWR hot leg, and to examine the effects of various geometrical parameters such as (1) the pipe diameter, (2) the length of horizontal pipe, and (3) the horizontal pipe length-to- diameter ratio on the CCFL.

## **2. EXPERIMENTS**

A series of experiments were performed and a total of 103 experimental data for the onset of CCFL and zero penetration (90 for the onset of CCFL and 13 for the zero penetration) in the simulated PWR hot leg have been obtained for various combinations of test parameters.

### **2.1 EXPERIMENTAL APPARATUS**

A schematic of the experimental apparatus is shown in Fig. 1(a). The experimental loop was designed to form a countercurrent flow in a test section. Water and air were used as the working fluids. The main components of the system were (a) the test section, (b) the air supply, (c) the water circulation system, and (d) the instrumentation and data acquisition system. A total of 8 different test sections (with different combinations of the pipe diameter, the horizontal pipe length, and the inclined riser as summarized in Table 1) were made of transparent acrylic glass to allow visual observation of the flow pattern. Each test section consisted of a horizontal pipe connected to an inclined riser by a 35° bend as shown in Fig. 1(b). The inner and outer radii of the curvature of the bend were 40 and 80 mm for the 40 mm bore pipe and 80 and 160 mm for the 80 mm bore pipe, respectively. The bends with different inner diameter were carefully constructed by bending straight acrylic glass pipes while they were heated on a machined die.

One end of the horizontal pipe was connected to the air vessel, while the other end of the inclined riser was connected to the water vessel. The air vessel had a cubic shape (600 × 600 × 1000 mm) and

the water vessel had a rectangular cross-section ( $400 \times 400$  mm) with 805 mm height. As can be seen in Fig. 1(a), the water vessel had inclined wall in the upper region to be connected to the inclined riser of the test section.

Air was supplied from the roots-type blower (whose capacity was 0 ~ 6000 LPM and the maximum operation pressure was 1.3 bar) to pass through the pressure regulator, rotameters (with two different ranges), the air vessel and the test section. The water was pumped from the constant head water surge tank and passed through the magnetic flowmeter, the water vessel, the test section, and two water collection tanks. Thus, the water flow was countercurrent to the air and formed a closed loop. The flow rates of water and air were controlled not only by adjusting motor controllers of the water pump and the air blower, but also by opening the bypass valves installed on each supply lines.

A digital video camera with a speed of 30 frames per second was also used to photograph the flow pattern in the test section. A Hewlett Packard 3852A data acquisition unit (DAU) was used to process the output signals of transmitters and compensated type-K thermocouples. The Pentium processor PC controlled the HP 3852A DAU and recorded the data in the hard disk. Communication between the PC and the HP 3852A DAU was carried out via the HP-IB interface card.

## **2.2 TEST PARAMETERS & TEST PROCEDURE**

The controllable test parameters in the present work were (a) the pipe diameter, (b) the length of horizontal pipe, (c) the length of inclined riser, (d) the inlet flow rate of water, and (e) the inlet flow rate of air. A total of 103 runs were made for various combinations of test parameters using 8 different test sections under atmospheric pressure and room temperature conditions as summarized in Table 2. The ranges of superficial velocities of water and air (i.e.,  $j_L$  and  $j_G$ ) were 0.0133 ~ 0.2255 m/s and 0.7958 ~ 6.1009 m/s for the 40 mm diameter pipe and 0.0033 ~ 0.3747 m/s and 0.3316 ~ 9.2840 m/s for the 80 mm diameter pipe, respectively.

The experimental procedure with a given test section is as follows: (a) The inlet water flow rate was first set to a specified value. (b) The air flow rate was then increased in small steps until the onset of CCFL or the zero penetration limit occurred depending on the purpose of the test. (c) The void fraction was also measured at the point where the water depth was highest concurrently with each step of the air flow rate. The onset of CCFL was readily determined by visual observation as a slight increase in air flow rate (at the onset of CCFL) resulted in a dramatic change in the flow pattern and it was also confirmed by the sudden increment of pressure drop measured across the test section. In addition, the reproducibility of the present test data has been confirmed by repeating the same test three times under typical test conditions.

### 3. RESULTS AND DISCUSSION

#### 3.1 Three Categories of CCFL and CCFL Mechanisms Observed in Three Different Regions of Inlet Water Flow Rates

##### (1) Three Categories of CCFL

Figure 2 shows the major characteristic of pressure drop when the onset of CCFL occurred. According to the water flow rate that can exist in the test section for a given inlet water flow rate, the CCFL phenomenon can be classified into three different categories as shown in Fig. 3: ① the onset of CCFL, ② the partial delivery of water, and ③ the zero liquid penetration. As can be seen in Fig. 3, the point where the onset of CCFL occurred (i.e., the  $j_G^{*0.5}$  value for a given  $j_L^{*0.5}$  denoted by a dotted line in Fig. 3) varies depending on the inlet water flow rate. The zero liquid penetration limit for a given inlet water flow rate (denoted by small black circles on a solid line in Fig. 3), on the other hand, is almost constant implying that the zero liquid penetration limit is independent of the inlet water flow rate.

##### (2) CCFL Mechanisms Observed in Three Different Regions of Inlet Water Flow Rates

Figure 4 is a typical onset of CCFL curve (obtained with Test Section No.2: L=2000 mm, D=80 mm, Inclined Riser Legnth=623 mm, and  $\theta=35^\circ$ ) expressed in terms of Wallis flooding parameter ( $j_K^{*0.5}$ ) defined by

$$j_K^* = j_K \left[ \frac{\rho_K}{gD(\rho_L - \rho_G)} \right]^{0.5} \quad (1)$$

where  $j_K$  and  $\rho_K$  are the superficial velocities and densities of phase K ( L = liquid phase and G = gas phase), D is the diameter of the pipe, and g is the gravitational acceleration.

It may be recalled here that in an open channel flow, flows at depths greater than critical are known as subcritical flows; flows at depths less than critical are known as supercritical flows. When a change from supercritical to subcritical flow occurs in an open channel flow, a hydraulic jump appears. As a result, the water depth increases abruptly in the direction of flow. Although the expression that corresponds to the critical flow condition for stratified two-phase flow is different from that applicable to an open channel flow, the same terms are used to describe the stratified two-phase flow in the following.

As shown in Fig. 4, the CCFL curve can be divided into three regions based on the range of the inlet water flow rate (or equivalently,  $j_L^{*0.5}$ ). The observed mechanisms of CCFL in each region were

different depending on the inlet water flow rate as follows:

1). In the low water flow rate region (Region I:  $j_L^{*0.5} = 0 \sim 0.2$ ), the air flow rate to initiate the onset of CCFL decreased as the inlet water flow rate was increased. Due to the acceleration of water by gravity while flowing down through the inclined pipe, the supercritical flow suddenly changes to the subcritical flow at a certain location in the horizontal pipe and a hydraulic jump occurred at the flow transition point as shown in Fig. 5. The location of the hydraulic jump depended on the water flow rate: When the inlet water flow rate was decreased, the location of the hydraulic jump moved closer to the bend. As the inlet water flow rate was increased, the hydraulic jump moved away from the bend and the magnitude of hydraulic jump was also increased. Also, as the air flow rate was increased for a given inlet water flow rate, the hydraulic jump moved toward the bend and the air-water interface became very wavy. When the hydraulic jump arrived near the bend, the flow pattern became chaotic and oscillatory, and large roll waves were also observed at the air-water interface near the bend. Figure 6 shows the flow pattern observed in the vicinity of the bend when the CCFL occurred.

2). In the intermediate inlet water flow rate region (Region II:  $0.2 < j_L^{*0.5} < 0.4$ ), the air flow rate to initiate the onset of CCFL increased as the inlet water flow rate was increased. The accelerated water flowing down through the inclined pipe connected by a  $35^\circ$  bend maintained a supercritical flow throughout the horizontal pipe and no hydraulic jump occurred within the pipe. When the air flow rate reached the point of the onset of CCFL, the depth of water layer increased at the horizontal pipe outlet. At the same time, a large number of small water droplets were entrained in the upper region of the pipe from the air-water interface and also large amplitude roll waves were developed near the horizontal pipe outlet as can be seen in Fig. 7. These roll waves were moved quickly toward the bend by the flowing air. This, in turn, increased the velocity of air because of the decrease of the effective cross-sectional area of air flow by the roll waves. As a result of the increased air flow velocity, the water flow rate was eventually restricted.

3). In the high inlet water flow rate region (Region III:  $0.4 < j_L^{*0.5} < 0.7$ ), the air flow rate to initiate the onset of CCFL decreased as the inlet water flow rate was increased and it was independent of the test section geometry for a given pipe diameter. In the region III, there was no hydraulic jump in the horizontal pipe and also there was no increase of water layer depth at the horizontal pipe outlet. However, the onset of CCFL occurred at the inlet of the inclined pipe connected to the water vessel due to an active entrainment of water droplets into the water vessel.

It should be noted, however, the above quantitative criteria used to define the three different regions of the inlet water flow rate are not directly applicable to other test sections with a different combination of pipe geometry such as L, D, and L/D.

### 3.2 Effects of Various Geometrical Parameters on CCFL

#### (1) Pipe Diameter Effect on CCFL

To examine the effect of the pipe diameter on the CCFL, experimental data obtained with four different combinations of pipe diameter and horizontal pipe length are plotted in Fig. 8. A comparison between curves (a) and (b) shows that the effect of pipe diameter on the onset of CCFL for short horizontal pipes ( $L = 928$  and  $700$  mm) is not clear. For longer horizontal pipes ( $L = 3388$  mm), curves (c) and (d), on the other hand,  $j_G^{*0.5}$  values to initiate the onset of CCFL for smaller pipe diameter ( $D = 40$  mm) are much smaller than that for larger pipe diameter ( $D = 80$  mm) for a given value of  $j_L^{*0.5}$ .

#### (2) Horizontal Pipe Length Effect on CCFL

The CCFL data obtained with test sections of three different horizontal lengths are shown in Fig. 9. This figure clearly shows that a longer horizontal pipe length leads to lower velocities of air and water for the onset of CCFL which agrees with the results of others. As already pointed out by earlier workers (Ohnuki, 1986; Siddiqui et al., 1986; Wongwises, 1996), the longer horizontal pipe lengths cause the water level to be higher in the vicinity of the bend due to an increase in frictions at the wall and interface and slows down the water flow. This in turn induces a higher gas velocity and hence an earlier formation of unstable wave growth at the hydraulic jump.

#### (3) Length-to-Diameter Ratio (L/D) Effect on CCFL

To examine the effect of the horizontal pipe length-to-diameter ratio, flooding parameters,  $j_L^{*0.5}$  versus  $j_G^{*0.5}$ , are plotted using  $L/D$  as a major parameter in Fig. 10. This figure also shows that a larger  $L/D$  leads to lower velocities of air and water for the onset of CCFL. That is, the onset of CCFL occurs at consistently lower flow rates when the  $L/D$  is increased. Since a larger  $L/D$  corresponds to a longer horizontal pipe length for a given pipe diameter, the same reasoning used in the horizontal length effect on the CCFL is applicable.

## 4. SUMMARY AND CONCLUSIONS

Experiments have been performed to examine the effects of various geometrical parameters, such as the pipe diameter, the length of horizontal pipe, and the horizontal pipe length-to-diameter ratio, on the air-water CCFL in a simulated PWR hot leg. A total of 103 experimental data for the onset of CCFL and zero liquid penetration (i.e., 90 for the onset of CCFL and 13 for the zero liquid penetration) have been obtained for various combinations of test parameters. The results of present experiments can be

summarized as follows:

According to the water flow rate that can exist in the test section for a given inlet water flow rate, the CCFL phenomenon can be classified into three different categories: ① the onset of CCFL, ② the partial liquid delivery, and ③ the zero liquid penetration.

The observed mechanisms of CCFL were different depending on the inlet water flow rate. The effect of pipe diameter on the onset of CCFL for short horizontal pipes ( $L = 700$  and  $928\text{mm}$ ) is not evident. For longer horizontal pipes ( $L = 3388$  mm) with a small pipe diameter ( $D = 40$  mm), however, air flow rates ( $j_G^{*0.5}$  values) to initiate the onset of CCFL are much smaller than that with a larger pipe diameter ( $D = 80$  mm) when the inlet water flow rate ( $j_L^{*0.5}$  values) is fixed. The effects of horizontal pipe length ( $L$ ) and horizontal pipe length-to-diameter ratio ( $L/D$ ) on CCFL are about the same: a longer horizontal pipe length (or a larger  $L/D$ ) leads to lower velocities of air and water for the onset of CCFL.

**Table 1 Test Section Geometry of the Present Experiments**

Volume Reduction Ratio	Inner Pipe Diameter (D) (mm)	Horizontal Pipe Length (L) (mm)	Inclined Riser Length (I) (mm)	Inclination Angle ( $\theta$ ) (deg.)	Test Section Number
1 / 650	80	928 ( *12)	623	35	No.1
		2000 ( *25)			No.2
		3388 ( *42)			No.3
		3388 ( *42)	0	No.4	
		3388 ( *42)	0	No.5	
1 / 3675	40	700 ( *18)	648	35	No.6
		1000 ( *25)			No.7
		3388 ( *85)			No.8

\* L/D Ratio

**Table 2 Test Matrix of the Present Experiments**

Test Section	Water Flow Rate (LPM)	Air Flow Rate (LPM)	$j_L$ (m/s)	$j_G$ (m/s)	Test No.	No. of Data
No.1 No.2 No.3 No.4 No.5	1, 3, 6, 11, 17, 24, 33, 43, 54, 67, 81, 96, 113	100 ~ 2800 1 Step : 25	0.0033 ~ 0.3747	0.3316 ~ 9.2840	No.1-1 : :	73
No.6 No.7 No.8	1, 2, 3, 4, 6, 8, 10, 12, 14, 17	60 ~ 460 1 Step : 10	0.0133 ~ 0.2255	0.7958 ~ 6.1009	No.6-1 : :	30
<b>Total Number of Experimental Data</b>						<b>103</b>

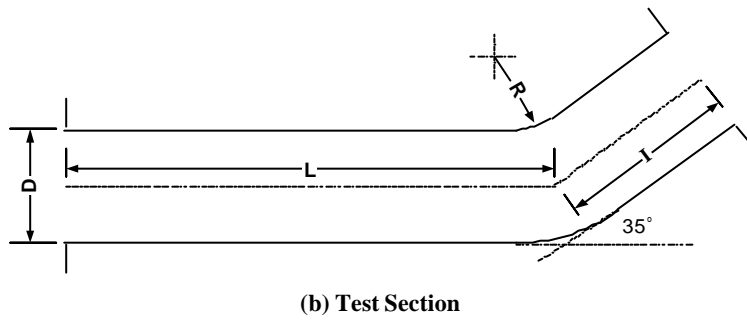
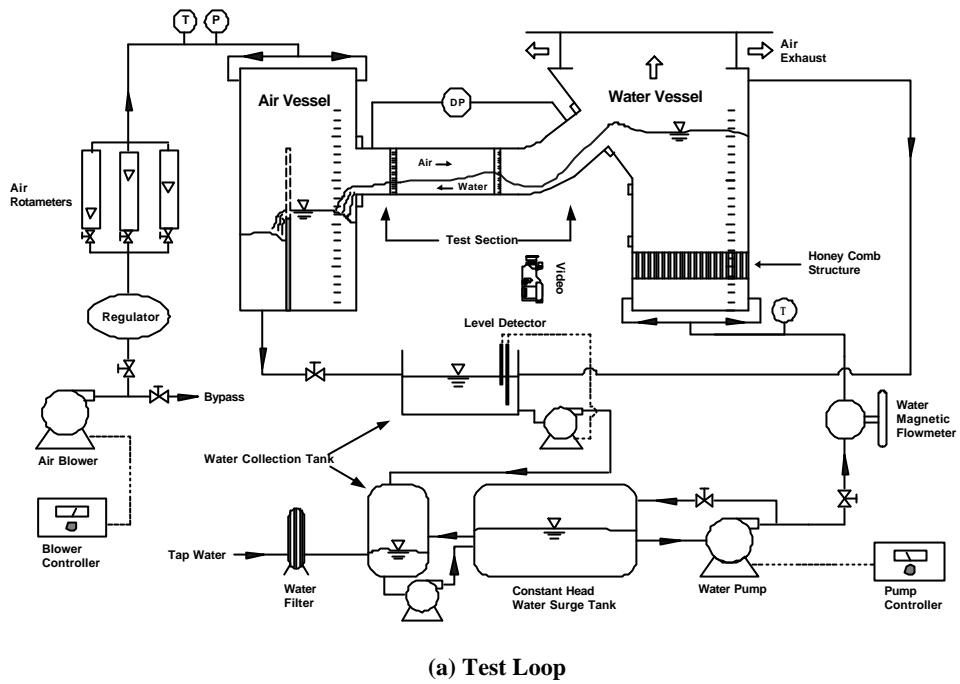


Fig. 1 Schematic Diagram of Experimental Apparatus

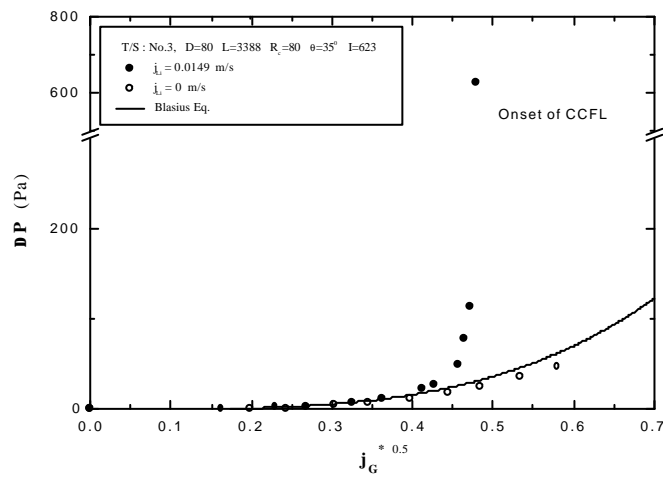
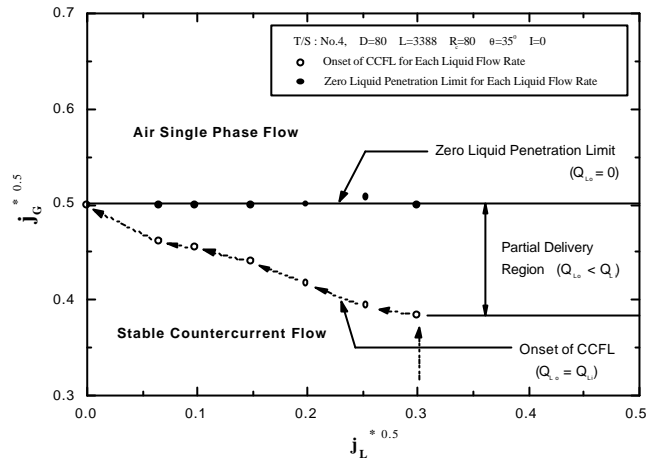
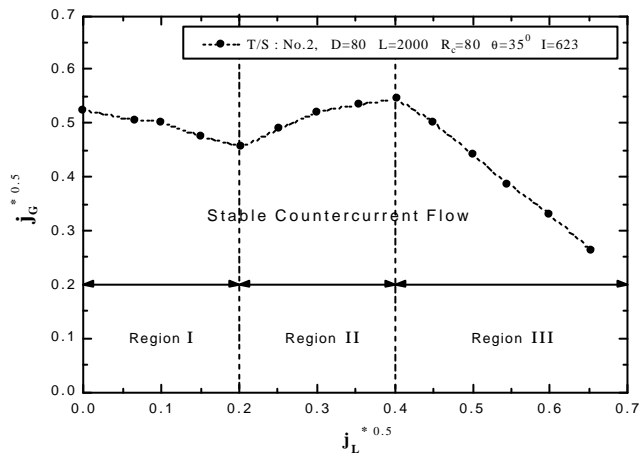


Fig. 2 Relationship between Pressure Drop and Air Flow Rate at Constant Inlet Water Flow Rate



**Fig. 3 Three Categories of CCFL**



**Fig. 4 Typical Onset of CCFL Curve**



**Fig. 5 Hydraulic Jump in the Horizontal Pipe ( $j_L^* 0.5 < 0.2$ )**



Fig. 6 Water Hold Up at the Bend When the CCFL Occurs ( $j_L^{*0.5} < 0.2$ )



Fig. 7 The Large Roll Wave Formation at the Outlet of Water ( $j_L^{*0.5} = 0.2 \sim 0.4$ )

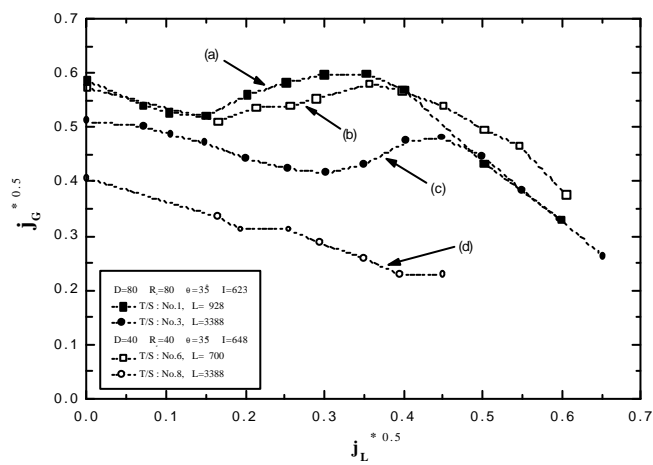
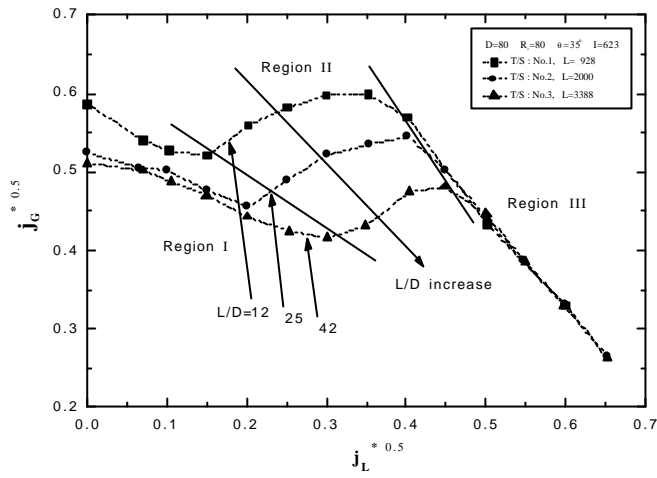
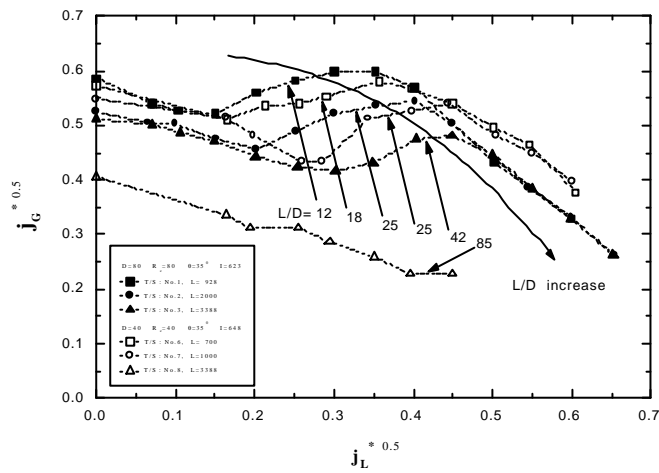


Fig. 8 Effect of Pipe Diameter on CCFL



**Fig. 9 Effect of Horizontal Pipe Length on CCFL**



**Fig. 10 Effect of Horizontal Pipe Length-to-Diameter Ratio on CCFL**

### ACKNOWLEDGEMENT

The authors gratefully acknowledge the financial support of Korea Electric Power Research Institute (KEPRI) provided for this work.

### REFERENCES

A. Ohnuki, "Experimental Study of Counter-Current Two-Phase Flow in Horizontal Tube Connected to Inclined Riser," *J. Nucl. Sci. Tech.*, Vol. 23, No. 3, pp. 219-232, 1986.

- G. B. Wallis, "One-Dimensional Two-Phase Flow," *McGraw-Hill*, 1969.
- G. B. Wallis and J. E. Dobson, "The Onset of Slugging in Horizontal Stratified Air-Water Flow," *Int. J. Multiphase Flow*, Vol. 1, pp. 173-193, 1973.
- G. C. Gardner, "Flooded Countercurrent Two-Phase Flow in Horizontal Tubes and Channels," *Int. J. Multiphase Flow*, Vol. 9, No. 4, pp. 367-382, 1983.
- H. Siddiqui, S. Banerjee, and K. H. Ardron, "Flooding in an Elbow Between a Vertical and a Horizontal or Near-Horizontal Pipe," *Int. J. Multiphase Flow*, Vol. 12, No. 4, pp. 531-541, 1986.
- K. Y. Choi and H. C. No, "Experimental Studies of Flooding in Nearly Horizontal Pipes," *Int. J. Multiphase Flow*, Vol. 21, No. 3, pp. 419-436, 1995.
- M. Kawaji, L. A. Thomson, and V. S. Krisnan, "Countercurrent Flooding in Vertical-to-Inclined Pipes," *Exp. Heat Transfer*, Vol. 4, pp. 95-110, 1991.
- S. S. Kutateladze, "Elements of the Hydrodynamics of Gas-Liquid Systems," *Fluid Mech.-Sov. Res.*, Vol. 1, No. 4, pp. 29-50, 1972.
- S. Wongwises, "Two-Phase Countercurrent Flow in a Model of a Pressurized Water Reactor Hot Leg," *Nucl. Eng. Des.*, Vol. 166, pp. 121-133, 1996.